physica status solidi a
www.pss-a.com

Determination of the Complex Refractive Index of $GaSb_{1-x}Bi_x$ by Variable-Angle Spectroscopic Ellipsometry

*John McElearney, Kevin Grossklaus, T. Pan Menasuta, and Thomas Vandervelde**

Variable-angle spectroscopic ellipsometry is used to determine the room temperature complex refractive index ($\tilde{n} = n + ik$) of molecular beam epitaxy grown $GaSb_{1-x}Bi_x$ films with $x \leq 4.25\%$ over a spectral range of 0.47–6.2 eV. By correlating to critical points in the extinction coefficient k, the energies of several interband transitions are extracted as functions of Bi content. The observed change in the fundamental bandgap energy (E_0, −36.5 meV per %Bi) agrees well with previously published values; however, the samples examined here show a much more rapid increase in the spin-orbit splitting energy (Δ_0, +30.1 meV per Bi) than previous calculations have predicted. As in the related GaAsBi, the energy of transitions involving the top of the valence band are observed to have a much stronger dependence on Bi content than those that do not, suggesting the valence band maximum is most sensitive to Bi alloying. Finally, the effects of surface droplets on both the complex refractive index and the critical point energies are examined.

Key Points: GaSbBi films with ≤4.25% Bi are grown by molecular beam epitaxy. Their refractive indices are determined by variable-angle spectroscopic ellipsometry. Energies for a slew of interband transitions are extracted from these spectra. The measured bandgap reduction rate (−36.5 meV per %Bi) agrees well with literature measuring by other techniques. Spin-orbit splitting increases with Bi, which is expected to lead to a suppression of Auger recombination. The strong Bi dependency of transitions involving the valence band maximum, relative to those that do not, suggests the valence band is most sensitive to Bi alloying.

1. Introduction

Dilute III–V-bismide alloys, such as $GaSb_{1-x}Bi_x$, have garnered increased interest in recent years for their potential use in infrared optoelectronic devices. The energy of the Bi impurity state relative to the host valence band edge results in an anticrossing interaction that dramatically reduces the resulting alloy's bandgap energy.[1] In $GaSb_{1-x}Bi_x$, reductions of up to 36 meV per %Bi[2] have been observed at dilute concentrations (for $x \leq 8\%$), though this rate decreases as Bi fraction increases.[3] Additionally, a second anticrossing interaction has been predicted to increase the material's spin-orbit splitting energy Δ_0[4]—the separation of the valence band maximum and the split-off band at the gamma point. It has been proposed that when the spin-orbit splitting energy becomes greater than the bandgap energy, Auger recombination may be suppressed.[5,6] Given the disproportionate impact of Auger recombination on devices made of low-bandgap materials,[7] this could be of great benefit to III–V-Bi-based optoelectronics.[8] These factors, combined with the already shallow bandgap of GaSb ($E_0 = 0.72$ eV[9]) and the ability to grow these films pseudomorphically on commercially available substrates, make $GaSb_{1-x}Bi_x$ a prime candidate for use in mid- to far-infrared optoelectronic devices.

Effective design of such devices will require a fuller understanding of the effect Bi has on the host optical properties. To date, characterization of $GaSb_{1-x}Bi_x$ has focused primarily on the change in the fundamental bandgap energy E_0. Since the first demonstration of low-Bi-content, liquid-phase epitaxy-grown GaSbBi,[10] photoluminescence has been the most common technique for determining bandgap.[2,11] In addition to tracking the change in bandgap energy, photoreflective measurements have been employed to look at changes in the temperature variance of E_0 with increasing Bi[12] as well as to model changes in the electronic band structure, including predicted changes to the split-off band.[13] Fourier-transform infrared spectroscopy has been used to measure sub-bandgap absorption[14,15] down to 0.05 eV; however, experimental work looking away from the bandgap remains limited.

Spectroscopic ellipsometry (SE) presents an opportunity for more robust optical characterization, allowing for the determination of the complex refractive index, in addition to the absorption coefficient, over a wide spectral range. SE has previously been used to great effect for a wide set of III–V binaries[16] and their related alloys, most notably for this work GaSb and $GaAs_{1-x}Bi_x$. In GaSb, room temperature measurements have been made for energies ranging from 0.3 to 5.3 eV,[17] with additional work examining the effect of temperature over a more confined window, 1.4–5.6 eV.[18] An extensive study looking at the effect of Bi on optical properties in $GaAs_{1-x}Bi_x$[19] covered a spectral window

J. McElearney, K. Grossklaus, T. P. Menasuta, T. Vandervelde
Department of Electrical and Computer Engineering
Tufts University
Medford, MA 02155, USA
E-mail: tvanderv@ece.tufts.edu

The ORCID identification number(s) for the author(s) of this article can be found under https://doi.org/10.1002/pssa.202400017.

DOI: 10.1002/pssa.202400017

of 0.37–9.1 eV for films with wide range of Bi fraction, $x \leq 17\%$. Additionally, these studies all show that inferences into the material band structure can be made by correlating critical points (CPs) in the measured dielectric function to interband transitions. These techniques have also been applied to the $Tl_xGa_{1-x}As$ material system,[20] as well as certain Group-IV alloys, such as GeSn.[21]

In this article, we report room temperature optical constants for $GaSb_{1-x}Bi_x$ as functions of Bi content and incident photon energy as determined by variable-angle SE. Specifically, values for the refractive index n, the extinction coefficient k, and the absorption coefficient α were measured over an energy range of 0.47–6.2 eV (200 nm–2.60 μm) for $GaSb_{1-x}Bi_x$ films with $x \leq 4.25\%$. From these, the energies of key interband transitions, such as the fundamental bandgap (E_0) and split-off band energy ($E_0 + \Delta_0$), were determined as functions of Bi content by CP analysis of the second derivative of k with respect to energy. Lastly, some early observations into the effects of surface droplets on optical behavior are discussed.

2. Experimental Section

Samples were grown by solid-source molecular beam epitaxy (MBE) on unintentionally doped, (100) oriented GaSb substrates in a Veeco GENxplor chamber. Ga and Bi fluxes were supplied by high-temperature effusion cells, while a valved cracker cell was used for Sb. Source fluxes were monitored via beam equivalent pressures (BEP) before growth using a N_2 calibrated ion gauge. Reflection high-energy electron diffraction (RHEED) was used to monitor surface conditions before and during growth, as well as measuring GaSb growth rates via Ga RHEED intensity oscillations and determining the Ga:Sb BEP ratio at the GaSb stoichiometric point at growth temperatures. Temperatures above ≈400 °C were monitored by a combination of blackbody emission spectroscopy and optical pyrometry using a k-Space Associates BandiT spectrometer and a BASF Exactus optical pyrometer, respectively. For lower temperatures, a trend correlating substrate heater setpoint to measured frontside temperature was established and extrapolated down. To do so, the substrate heater temperature was lowered in 25 °C steps until the Blackbody spectrometer reached its low-temperature limit. Temperatures reported here are frontside, growth surface temperatures unless otherwise noted.

GaSb substrates were heated under Sb overpressure to ≈545 °C in order to desorb the epiready oxide. The sample was then cooled to 490 °C, and a 500 nm GaSb buffer was grown at 0.25 ML s^{-1}. The Ga flux was chosen to control growth rate, while the Sb flux was set 20% above the stoichiometric condition to achieve the smoothest possible starting surface for the Bi-containing layers. Following buffer growth, the sample was cooled to the $GaSb_{1-x}Bi_x$ target growth temperature of 295 °C. During cooldown, the Sb shutter was closed once the sample reached ≈380 °C to prevent excess Sb deposition on the surface. For the $GaSb_{1-x}Bi_x$ layers, the Sb flux was reduced to exactly match the GaSb stoichiometric ratio, while the Bi flux was adjusted to vary Bi content. All GaSbBi films were grown to 100 nm thick, at a growth rate of 0.25 ML s^{-1}.

Surface morphology was characterized by a combination of Nomarski optical microscopy and atomic force microscopy (AFM). Nomarski was used to qualitatively identify any large surface features, such as the metallic droplets that can occur during III–V-Bi growth,[22] while AFM was used to measure surface roughness and, whether they were present, droplet size, and density. Of the samples discussed here, only the highest Bi content film ($x = 4.25\%$) was found to have formed droplets.

Sample composition and film thickness were determined primarily by high-resolution X-ray diffraction (HRXRD) using a Bruker D8 diffractometer. To deconvolute the effects of Bi incorporation and strain on the out-of-plane lattice constant, both symmetric, $2\theta/\omega$ (004) line scans and glancing exit (224) reciprocal space maps were taken. For this purpose, all GaSbBi films were assumed to have the same elastic moduli and Poisson's ratio as GaSb.[23] As seen in **Figure 1**, all samples showed clear Pendellösung fringes which, while somewhat broad, indicated good compositional homogeneity throughout the films. Likewise, reciprocal maps confirm that GaSbBi films grew psuedomorphically to the GaSb substrate. Even the sample with surface droplets shows no signs of phase separation, which has been observed following droplet formation in related material sets.[24,25]

As a technique, SE uses a measured change in the polarization state of light after reflecting off a sample to determine the material's optical constants. Monochromatic light was first passed through a polarizer, splitting the signal into a known combination of s- and p-polarized light. As these will reflect off the sample differently based on the materials' optical constants; the ratio of the reflected signals, normalized to their initial values, can be used to determine what those constants are. This ratio, denoted ρ, is defined as

$$\rho = \frac{E_{r,p}/E_{i,p}}{E_{r,s}/E_{i,s}} = \frac{r_p}{r_s} = \tan(\psi)e^{i\Delta} \quad (1)$$

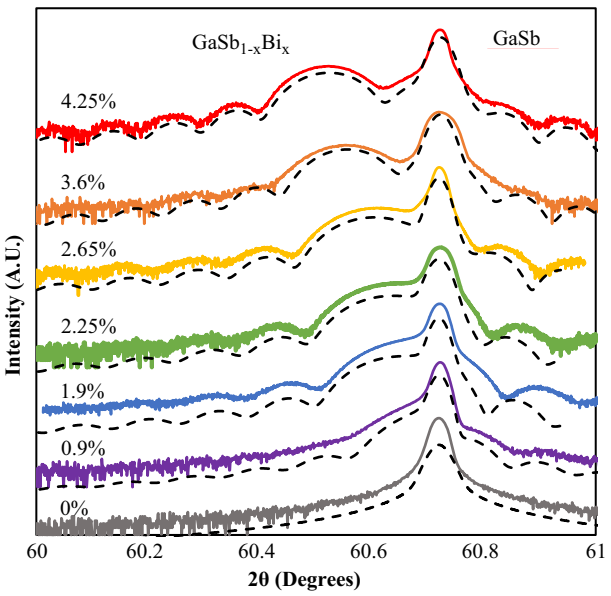

Figure 1. HRXRD $2\theta/\omega$ (004) line scans for $GaSb_{1-x}Bi_x$ samples with x ranging from 0 to 4.25%. Dashed curves represent simulated fits. The highest Bi fraction film, $x = 4.25\%$ (red), formed surface droplets, but the clear Pendellösung fringes still indicate good film homogeneity.

where $\tan(\Psi)$ is the ratio of the normalized amplitudes of the reflected p- and s-polarized signals and Δ is the phase difference between the two. Then, by treating the entire sample stack as a single-bulk material, these ellipsometric angles were converted to a complex pseudodielectric function ($\varepsilon = \varepsilon_1 + i\varepsilon_2$) by the relationship[26]

$$\varepsilon = \sin^2(\phi) * \left[1 + \tan^2(\phi) * \left(\frac{1-\rho}{1+\rho}\right)^2\right] \quad (2)$$

where ϕ is the angle of incidence. Information about the complex dielectric function of a particular layer can be extracted from these pseudodielectric functions by fitting a layer-by-layer model to the measured spectra for ε_1 and ε_2. Ultimately, the extracted dielectric function for the layer of interest can be used to determine the complex refractive index given by

$$\varepsilon = \tilde{n}^2 \quad (3)$$

However, to extract information of an as-of-yet uncharacterized material, such as GaSbBi, requires knowing both thicknesses and optical constants for all underlayers. For these samples, thicknesses were determined by a combination of growth rate calculations and HRXRD measurements. To determine the optical constants for our underlayers, preliminary ellipsometric scans of an epiready undoped GaSb wafer with oxide desorbed under Sb overpressure in the MBE and of a homoepitaxial GaSb layer grown as described above were made in advance of the Bi-containing films. Separate models were required for each as our grown GaSb layers showed slightly different optical behavior from our substrates, likely due to a difference in background doping levels. To limit formation of an oxide layer on the GaSb surface, the desorbed wafer was loaded into a cryostat and held under vacuum ($<10^{-9}$ torr) immediately upon removal from the growth chamber: ≈15 min in air until fully pumped down. Room-temperature measurements of the desorbed GaSb wafer occurred under vacuum in the cryostat, while all other scans discussed were performed in air.

Measurements were made using a J.A. Woollam variable-angle spectroscopic ellipsometer (VASE), covering an energy range of 0.47–6.2 eV (200–2600 nm). Scans were taken at room temperature, at incident angles of 70° and 75°. For all Bi-containing samples, as well as the homoepitaxial GaSb buffer, the entire spectral range was scanned with a 10 meV step size. For the desorbed GaSb substrate, the scan was split into regions to allow finer resolution over key features in the dielectric function, most crucially over the bandgap, where a 1 meV step size was used.

For all samples, the model of the unknown layer was constructed from a series of adjustable oscillators modeled loosely on CPs in the dielectric function.[27] Parameters such as central energy, amplitude, and breadth were adjusted to produce the best fit to the measured pseudodielectric functions ε_1 and ε_2. The software used (WVASE) has the additional benefit of enforcing the Kramers–Kronig relation between n and k in the modeled spectra. As the properties of both the GaSb and GaSbBi oxide are not well known for the energy ranges of interest, all samples also included a Bruggeman effective medium approximation (EMA) as the surface layer. This is a 50/50 mixture of the immediate underlayer, in each case, the unknown layer and void, which has proven effective at modeling both surface oxides and roughness.[28] For the samples presented here, best results were obtained with an average EMA layer thickness of ≈2.8 nm. This was slightly higher than the average RMS roughness as determined by AFM, ≈1.0 nm; however, this was to be expected, as the EMA layer was accounting for the combined effect of both the oxide layer and any surface roughness.

Building up to the Bi-containing samples, the fit of the ellipsometric data for the GaSb wafer was constructed by just two layers, a 500 µm oscillator layer and several nanometers of the Bruggeman EMA layer. Once the model for the wafer was built, it was used as the bottom of the three-layer GaSb buffer stack—500 µm of GaSb Wafer, 500 nm of the oscillator layer, and a similarly thin Bruggeman EMA. In this case, when fitting the oscillators closest to the bandgap, some parameters of the GaSb wafer underlayer were also allowed to vary, as we have observed that the band edge of our underlayers sharpens significantly when they no longer contain any surface states. Once completed, the "buried" GaSb wafer and the GaSb buffer layer were carried over into the four-layer stack used for the Bi-containing samples, 500 µm of the "buried" GaSb wafer, 500 nm of the homoepitaxial GaSb buffer layer, ≈100 nm of the oscillator layer used to model the GaSbBi, and then 2–4 nm of the Bruggeman EMA layer to account for the surface roughness and oxide. As before, the oscillators of the GaSb buffer nearest to the bandgap were allowed to vary over a narrow range now that it was no longer the epilayer.

For all samples, fitting began by determining the thicknesses of both the unknown and the surface oxide layers. This was done by allowing both to vary around approximate starting points, taken either from growth rate estimates, HRXRD measurements, or known wafer thicknesses, and fitting to the transparent, sub-bandgap region of the imaginary part of the pseudodielectric function ε_2, ≈0.5–0.6 eV. Oscillators were then adjusted in order of increasing energy, starting, most critically, with those closest to the band edge, 0.5–1.0 eV. With those locked in, oscillators were then fit to the region around the observed split-off band, 1.0–2.0 eV; the E_1 and $E_1 + \Delta_1$ peaks, 2.0–3.0 eV; and ultimately, to the broader, high-energy E'_0, $E'_0 + \Delta'_0$, E_2 and E'_1 peaks, 3.0–6.2 eV. With a close fit achieved, all layer thicknesses and oscillator properties, with the exception of those nearest to the bandgap, were allowed to vary together to produce the closest fit. Finally, using this Kramers–Kronig consistent oscillator model as a starting point, optical constants n and k were adjusted to fit the measured pseudodielectric constants at each measured wavelength. This captured small features in the dielectric function, albeit at the cost of increased noise. All data presented in this article were obtained by such fitting.

The CP energies were then numerically extracted from these n and k spectra for GaSb and each GaSbBi film. A fifth-order Savitzky–Golay smoothing[29] was first applied to the fit spectra for the extinction coefficient k. Then numerical first and second derivatives, with respect to energy, of k were taken, from which the zero crossings at inflection points were used to identify the CP energies.

3. Results

The extracted n and k spectra for the full range of GaSbBi films, as well as for a bare GaSb wafer, are shown in **Figure 2**.

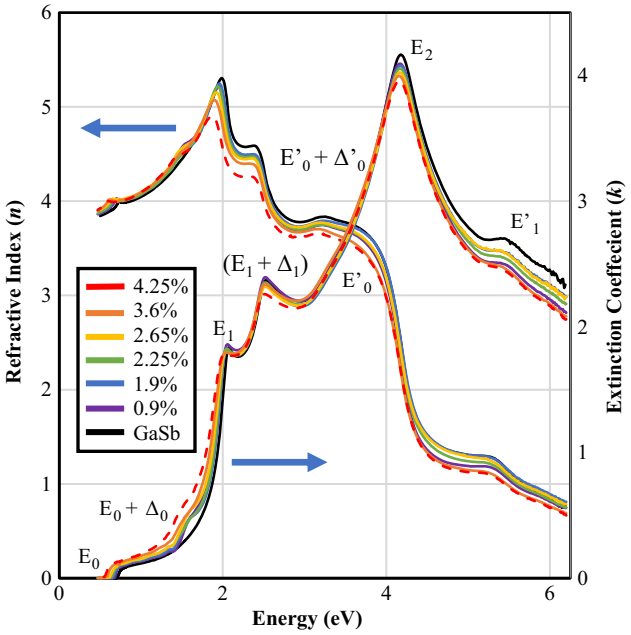

Figure 2. Extracted n and k spectra for $GaSb_{1-x}Bi_x$ films with x ranging from 0 to 4.25%. CPs in each spectrum are labeled with their corresponding interband transition. A dashed line is used to identify the sample with surface droplets present.

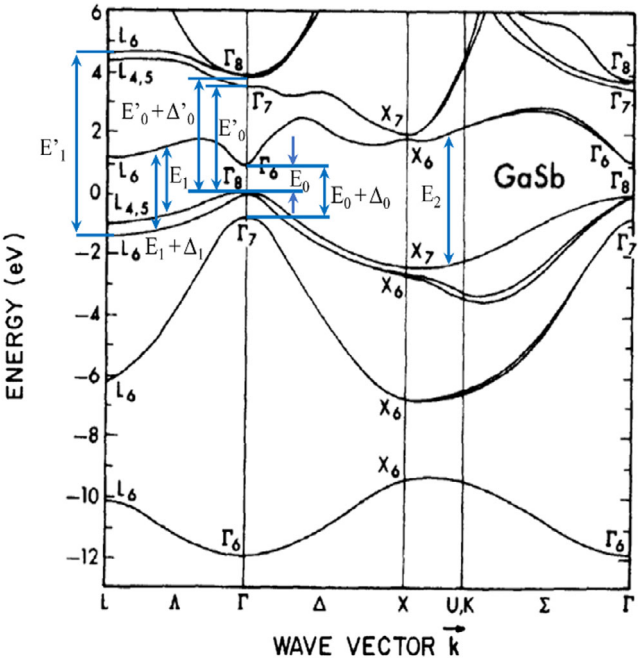

Figure 3. Calculated band structure for GaSb with interband transitions labeled. Original calculations by Chelikowsky and Cohen.[30] Reproduced with permission. Copyright 1976, American Physical Society. Transition labels adapted from Zollner et al.[18]

The results for our desorbed GaSb wafer show reasonably good agreement with previously reported values,[16–18] though we do observe a slight difference in the magnitude of both n and k. This difference is greatest near the E_2 peak (located at ≈4.5 eV) which is frequently used as a figure of merit for surface quality,[19] leading us to believe that any disagreement is likely due to differences in sample preparation. This is further evidenced by the thicker surface EMA layer required for our models (≈2.8 nm) compared to the GaSb oxide used by these earlier studies (0.5,[18] <2.4 nm[16]).

CPs in the dielectric function are labeled with their corresponding band transitions. Applying the work previously done for GaSb[18,30] (see **Figure 3**) to all samples herein, these include E_0, the fundamental bandgap energy ($\Gamma_8^v - \Gamma_6^c$); $E_0 + \Delta_0$, the transition from the split-off band to the conduction band at the gamma point of the Brillouin zone ($\Gamma_7^v - \Gamma_6^c$); the E_1 and $E_1 + \Delta_1$ peaks, corresponding to transitions from the heavy-hole ($\Lambda_{4,5}^v - \Lambda_6^c$) and light-hole ($\Lambda_6^v - \Lambda_6^c$) bands, respectively, to the conduction band along the Λ line; E'_0, the transition from the valence band maximum to the bottom of the first band above the conduction band ($\Gamma_8^v - \Gamma_7^c$), followed by the $E'_0 + \Delta'_0$ transition ($\Gamma_8^v - \Gamma_8^c$) to its accompanying split-off band; E_2, corresponding to the transition from the valence to the conduction band at the X point ($X_7^v - X_6^c$); and finally, the highest energy transition observed, E'_1, the transition from the valence band to the second conduction band at the L point on the edge of the Brillouin Zone ($L_6^v - L_6^c$).

Most visible in the extinction (**Figure 4**) and absorption coefficients ($\alpha = 4\pi k/\lambda$, **Figure 5**), the bandgap energy shows both the expected redshift and broadening with increasing Bi fraction. The small feature in k and α of the Bi-containing films at

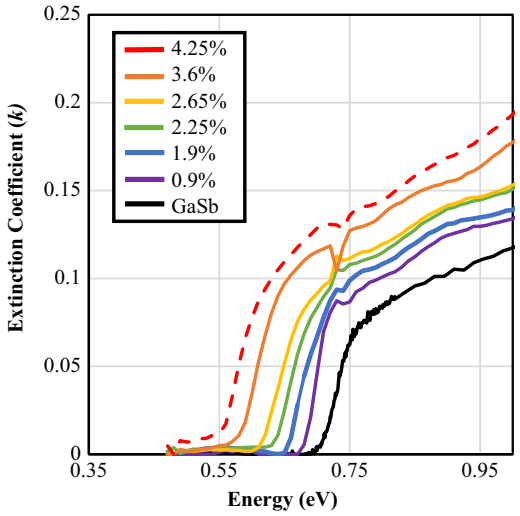

Figure 4. Extracted extinction coefficient k near the bandgap energy for the full range of GaSbBi films. Band edge shifts to lower energies with increasing Bi, while also showing a slight broadening at higher Bi content.

≈0.72 eV is believed to be an artifact from the final point-by-point fitting caused by the bandgap of the underlying GaSb substrate and buffer. The most dramatic effect of the Bi, however, is the emergence of the split-off peak at the $E_0 + \Delta_0$ energy in the region around 1.5 eV. While not visible at all in the GaSb wafer, this peak becomes immediately apparent in even the lowest Bi fraction GaSbBi film (**Figure 6**). This peak also shows a shift

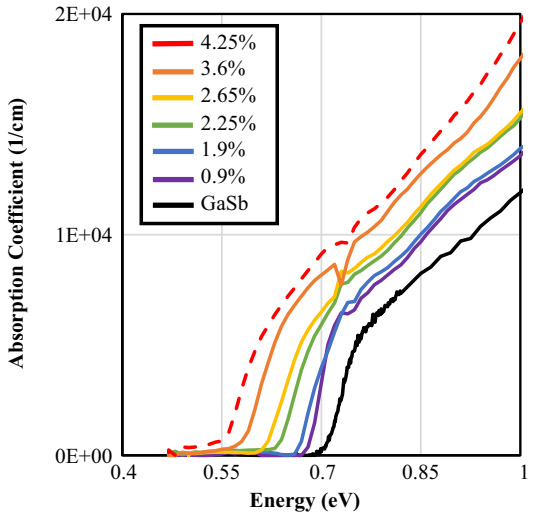

Figure 5. Absorption coefficient as a function of energy for energies nearest to the band edge. Bandgap energy shows the expected redshifting with increasing Bi content. The sample with surface droplets present ($x = 4.25\%$, red, dashed) exhibits a slightly longer Urbach tail,[34] indicating an increase in sub-bandgap absorption.

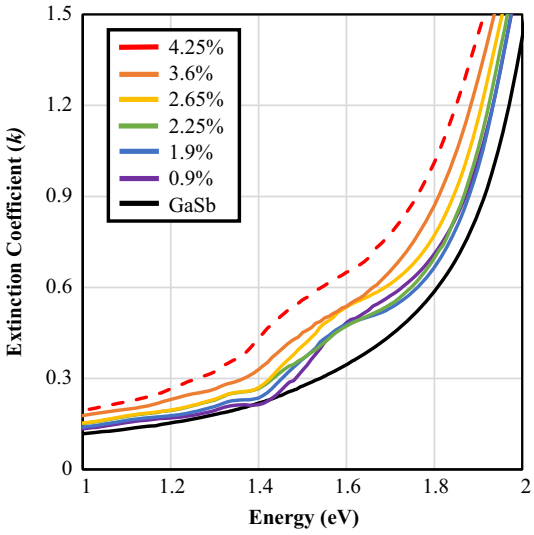

Figure 6. Extinction coefficient near the $E_0 + \Delta_0$ peak. This peak only becomes visible once Bi is present in the film.

to lower energy with increasing Bi content, but not quite as dramatically as the bandgap alone, implying an increase in the spin-orbit splitting energy with increasing Bi content.

Following the method described previously, CP energies were extracted from the numerical second derivative of the extinction coefficient. An example is shown in **Figure 7**. CP energies are plotted as functions of Bi content in **Figure 8**. Straight line fits are applied to each CP, including the bandgap energy, with trend lines labeled with their slopes in meV per %Bi. Fits are required to pass through the measured CP energies of GaSb at $x = 0$. As it is not clearly observable in our data, the value of Δ_0 for GaSb is

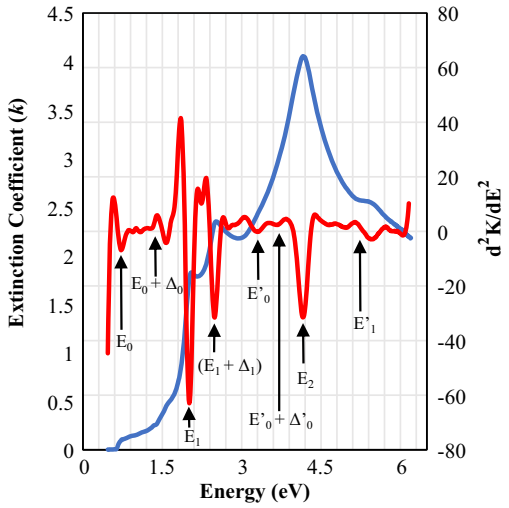

Figure 7. Representative overlay of the extinction coefficient (blue) and its second derivative (red) used to extract CP energies. The figure shown is for the sample with $x = 2.25\%$.

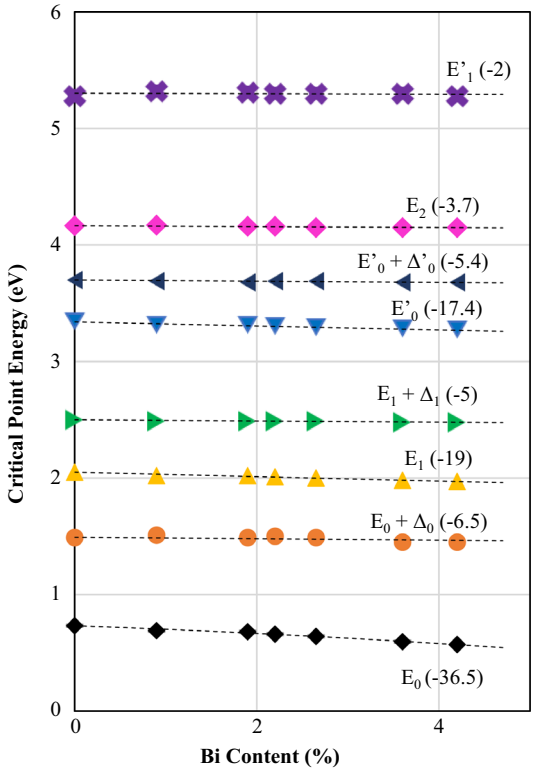

Figure 8. CP energies as functions of Bi content. Labels indicate the slopes of the trendlines in meV per %Bi.

taken to be 0.76 eV, as established in previously published work.[9,10,31]

We observe a bandgap energy reduction of −36.5 meV per %Bi, which is in good agreement with previously reported values.[2,3] Despite that, the location of the $E_0 + \Delta_0$ peak remains relatively constant (−6.4 meV per %Bi), signaling a nearly

commensurate increase in the spin-orbit splitting energy (+30.1 meV per %Bi), shown in **Figure 9**. This increase is significantly higher than recent calculations have predicted (+12 to 16 meV per %Bi).[4,13] Thus, while Δ_0 sits just above E_0 in GaSb, this difference increases rapidly with increasing Bi content. This would suggest that in addition to driving the bandgap further into the infrared, alloying Bi should also drive the suppression of Auger recombination in GaSbBi films; however, a dedicated study would be required to say so with confidence.

For GaAsBi,[19] the interband transitions involving the top of the valence band – E_0, E_1 and E'_0 – were observed to have a stronger Bi dependence than those that did not. We measure those changes in GaSbBi to be −36.5, −19.0, and −17.4 meV per %Bi respectively. These rates are significantly higher than those for the remaining CPs: $E_0 + \Delta_0$ (−6.5 meV per %Bi); $E_1 + \Delta_1$ (−5 meV per %Bi): $E'_0 + \Delta'_0$ (−5.4 meV per %Bi); E_2 (−3.7 meV per %Bi); and E'_1 (−2.0 meV per %Bi). In GaAsBi, this was attributed to Bi having a disproportionate effect on the valence band maximum, and these results would suggest the same is true in GaSbBi. The weak Bi dependence of the $E_0 + \Delta_0$ transition compared to E_0 most directly implies it is the valence band, and not the conduction band, moving with Bi incorporation. It is worth noting that this runs counter to previous calculations,[4,13] which have predicted that in GaSbBi it is in fact the conduction band minimum that is most sensitive to alloying.

For the purpose of comparison, we extrapolate these trends to estimate their values for the binary GaBi, and we compare them to values derived from various calculated band structures.[32,33] Additionally, we compare them to the results obtained from a similar ellipsometry study of GaAsBi,[19] which involved accompanying density functional theory (DFT) calculations. The linear extrapolation of the bandgap energy E_0 yields a value of −2.92 eV, displaying the expected semimetal behavior and in close agreement with the predicted −2.91 eV;[33] other calculations place it at −1.45 eV.[32] It should be noted that we expect our trend to overestimate the bandgap reduction, as the rate has been observed to diminish at higher Bi concentration.[3] For the weakly Bi-dependent CPs ($E_1 + \Delta_1$, $E'_0 + \Delta'_0$, E_2, and E'_1), we see good agreement with previously found values, particularly to the values extrapolated from GaAsBi.[19] The values are shown in **Table 1**.

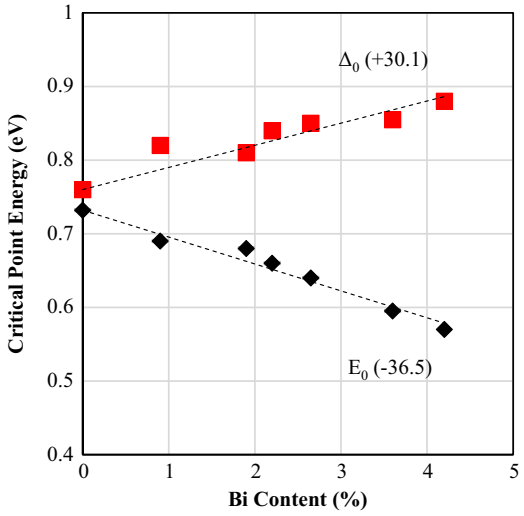

Figure 9. Bandgap (E_0) and spin-orbit splitting (Δ_0) energies as functions of Bi content. Labels indicate the slopes of the trendlines in meV per %Bi.

Table 1. Comparison of extrapolated and calculated CP energies (in eV) for the binary compound GaBi.

CP	GaBi (Extrapolated, GaSbBi)	GaBi (Extrapolated, GaAsBi[19])	GaBi (DFT[19])	GaBi[32]	GaBi[33]
E_0	**−2.92**	−3.68[a)]	−1.65	−1.45	−2.91
$E_1 + \Delta_1$	**2**[b)]	1.9	1.96	2.0	2.1
$E'_0 + \Delta'_0$	**3.16**	3.1	2.53	2.3	2.4
E_2	**3.79**	3.6	3.4–4.36	3.5–4.6	3.0–4.0
E'_1	**5.08**	5.5	4.50	4.6	3.2

[a)]Extrapolated from the linear approximation for the Bi dependence of the bandgap in GaAsBi.[19] [b)]Bold values highlight the work from this study.

Shifting focus to the sample with surface droplets present ($x = 4.25\%$), we observe a noticeable shift in both the refractive index and the extinction coefficient at lower energies, particularly near the $E_0 + \Delta_0$ peak. Additionally, the absorption coefficient displays a longer Urbach tail[34] than the other samples, indicating an increase in sub-bandgap absorption. Despite this, the extracted CP energies agree well with the trends established by the other samples examined. This, combined with the HRXRD results suggests the bulk homogeneity of GaSbBi may not be as sensitive to the presence of surface droplets as it is in GaAsBi.[25]

4. Conclusion

Through VASE, we have determined the complex refractive index for $GaSb_{1-x}Bi_x$ films with $x \leq 4.25\%$ over an energy range of 0.47–6.2 eV. From CPs in these spectra, we were able to extract the energies of a slew of interband transitions as functions of Bi content. Our measured bandgap reduction rate (−36.5 meV per %Bi) agrees well with literature values; however, we observe a much greater increase in the spin-orbit splitting energy (+30.1 meV per %Bi) than previous calculations have predicted. As there are no published values to compare to, we extrapolate our higher energy CP's to their value for the GaBi binary and find strong agreement with previous predictions. The rates of change of the interband transitions involving the top of valence band were found to be much higher than those that did not, suggesting Bi alloying primarily affects the valence band maximum. However, further characterization is required to draw a meaningful inference into the exact changes in the band structure. When surface droplets were present, we observed a shift in n and k at lower energies; however, CP energies continue to agree with trends established by the previous samples, suggesting that the bulk homogeneity of the film remained unaffected.

Acknowledgements

This work was supported by the Office of Naval Research (N00014-15-1-2946 and N00014-17-1-2591) and the National Science Foundation (ECCS 1930942, EECS 1806311, and ECCS 2120568). Samples were grown in the Tufts Epitaxial Core Facility on equipment supported by NSF EECS 1337783. This work was performed in part at the Harvard University Center for Nanoscale Systems (CNS), a member of the National Nanotechnology Coordinated Infrastructure Network (NNCI), which was supported by the National Science Foundation under NSF award no. ECCS-2025158. This work was carried out in part through the use of MIT.nano's facilities.

Conflict of Interest

The authors declare no conflict of interest.

Author Contributions

John McElearney was principally responsible for the design and execution of this experiment; grew the GaSbBi samples; performed X-ray diffraction measurements and analysis; performed variable-angle spectroscopic ellipsometry measurements, modeling and critical point extraction; analyzed data and created figures; and was the primary author of this article. **Kevin Grossklau** significantly contributed to the conceptualization of this experiment; assisted in the development of best practices for VASE measurement and modeling; wrote the MATLAB script required for critical point extraction; and provided valuable revision and editing during the drafting of this article. **T. Pan Menasut** took additional atomic force microscopy scans to help address reviewer comments. **Thomas Vandervelde** significantly contributed to the conceptualization of this experiment; advised in both data collection and analysis; provided all necessary resources, including equipment, source materials, and all associated funding; and provided insight over many revisions of this article.

Data Availability Statement

The data that support the findings of this study are available from the corresponding author upon reasonable request.

Keywords

III–V semiconductors, infrared photonics, molecular beam epitaxies, optoelectronics, refractive indices, spectroscopic ellipsometries

Received: January 15, 2024
Revised: May 26, 2024
Published online: July 23, 2024

[1] D. P. Samajdar, T. D. Das, S. Dhar, *Mater. Sci. Semicond. Process.* **2015**, *40*, 539.
[2] M. K. Rajpalke, W. M. Linhart, M. Birkett, K. M. Yu, J. Alaria, J. Kopaczek, R. Kudrawiec, T. S. Jones, M. J. Ashwin, T. D. Veal, *J. Appl. Phys.* **2014**, *116*, 043511.
[3] L. Yue, X. Chen, Y. Zhang, F. Zhang, L. Wang, J. Shao, S. Wang, *J. Alloys Compd.* **2018**, *742*, 780.
[4] S. Das, M. K. Bhowal, S. Dhar, *J. Appl. Phys.* **2019**, *125*, 075705.
[5] M. Takeshima, *J. Appl. Phys.* **1972**, *43*, 4114.
[6] S. J. Sweeney, Z. Batool, T. J. C. Hosea, S. R. Jin, presented at *First Int. Workshop on Bismuth Containing Semiconductors: Theory, Simulation, and Experiment*, Michigan **2010**.
[7] M. G. Mauk, in *Mid-Infrared Semiconductor Optoelectronics* (Ed: A. Krier), Vol. *118*, Springer, London **2006**, pp. 692–697.
[8] A. Zayan, M. Stevens, T. E. Vandervelde, in *Proc. IEEE 43rd Photovolt. Specialists Conf.*, Portland, OR **2016**, pp. 2839–2843.
[9] I. Vurgaftman, J. R. Meyer, L. R. Ram-Mohan, *J. Appl. Phys.* **2001**, *89*, 5815.
[10] S. K. Das, T. D. Das, S. Dhar, M. de la Mare, A. Krier, *Infrared Phys. Technol.* **2012**, *55*, 156.
[11] O. Delorme, L. Cerutti, E. Tournié, J.-B. Rodriguez, *J. Cryst. Growth* **2017**, *477*, 144.
[12] J. Kopaczek, R. Kudrawiec, W. M. Linhart, M. K. Rajpalke, K. M. Yu, T. S. Jones, M. J. Ashwin, J. Misiewicz, T. D. Veal, *Appl. Phys. Lett.* **2013**, *103*, 261907.
[13] M. P. Polak, P. Scharoch, R. Kudrawiec, J. Kopaczek, M. J. Winiarski, W. M. Linhart, M. K. Rajpalke, K. M. Yu, T. S. Jones, M. J. Ashwin, *J. Phys. D: Appl. Phys.*, **2014**, *47*, 355107.
[14] D. P. Samajdar, M. K. Bhowal, T. D. Das, S. Dhar, *J. Mater. Sci.: Mater. Electron.* **2016**, *27*, 8641.
[15] M. K. Bhowal, S. Das, A. S. Sharma, S. Dhar, *J. Electron. Mater.* **2019**, *48*, 5131.
[16] D. E. Aspnes, A. A. Studna, *Phys. Rev. B* **1983**, *27*, 985.
[17] M. Muñoz, K. Wei, F. H. Pollak, J. L. Freeouf, G. W. Charache, *Phys. Rev. B* **1999**, *60*, 8105.
[18] S. Zollner, M. Garriga, J. Humlíček, S. Gopalan, M. Cardona, *Phys. Rev. B* **1991**, *43*, 4349.
[19] M. Mahtab, R. Synowicki, V. Bahrami-Yekta, L. C. Bannow, S. W. Koch, R. B. Lewis, T. Tiedje, *Phys. Rev. Mater.* **2019**, *3*, 054601.
[20] S. Lenney, K. Grossklaus, M. Stevens, T. E. Vandervelde, in *Proc. SPIE*, San Francisco, CA **2019**, p. 10917.
[21] D. Imbrenda, R. A. Carrasco, R. Hickey, N. S. Fernando, S. Zollner, J. Kolodzey, *Appl. Phys. Lett.* **2021**, *119*, 162102.
[22] C. R. Tait, J. M. Millunchick, *J. Appl. Phys.* **2016**, *119*, 215302.
[23] A. Y. Vul', in *Handbook Series of Semiconductor Parameters* (Eds: M. Levinshtein, S. Rumyantsev, M. Shur), Vol. *1*, World Scientific, London **1996**.
[24] C. R. Tait, L. Yan, J. M. Millunchick, *Appl. Phys. Lett.* **2017**, *111*, 042105.
[25] M. A. Stevens, K. A. Grossklaus, T. E. Vandervelde, *J. Cryst. Growth* **2019**, *527*, 125216.
[26] J. A. Woollam, B. D. Johs, C. M. Herzinger, J. N. Hilfiker, R. A. Synowicki, C. L. Bungay, in *Proc. SPIE*, Vol. *10294*, San Francisco, CA **1999**, p. 3.
[27] M. Erman, J. B. Theeten, P. Chambon, S. M. Kelso, D. E. Aspnes, *J. Appl. Phys.* **1984**, *56*, 2664.
[28] G. E. Jellison, in *Handbook of Ellipsometry* (Eds: H. G. Tompkins, E. A. Irene), William Andrew Publishing, Norwich, NY **2005**.
[29] A. Savitzky, M. J. E. Golay, *Anal. Chem.* **1964**, *36*, 1627.
[30] J. R. Chelikowsky, M. L. Cohen, *Phys. Rev. B* **1976**, *14*, 556.
[31] C. Alibert, A. Joulliè, A. M. Joulliè, C. Ance, *Phys. Rev. B* **1983**, *27*, 4946.
[32] A. Janotti, S. H. Wei, S. B. Zhang, *Phys. Rev. B* **2002**, *65*, 115203.
[33] M. Ferhat, A. Zaoui, *Phys. Rev. B* **2006**, *73*, 115107.
[34] F. Urbach, *Phys. Rev.* **1953**, *92*, 1324.